ACS APPLIED MATERIALS & INTERFACES

Letter

www.acsami.org

One-Step Index-Tunable Antireflection Coatings from Aggregated Silica Nanoparticles

Kevin T. Cook,[†] Kwadwo E. Tettey,[‡] Robert M. Bunch,[∥] Daeyeon Lee,[‡] and Adam J. Nolte*[,†]

[†]Departments of Chemical Engineering and [∥]Physics and Optical Engineering, Rose-Hulman Institute of Technology, 5500 Wabash Avenue, Terre Haute, Indiana 47803, United States

[‡]Department of Chemical and Biomolecular Engineering, University of Pennsylvania, 220 South 33rd Street, Philadelphia, Pennsylvania 19104, United States

Supporting Information

ABSTRACT: We demonstrate a method for producing thickness- and refractive index-tunable antireflection coatings utilizing a one-step spin coating procedure with silica nanoparticle solutions. Aging nanoparticle solutions under controlled pH and temperature induces aggregation, allowing precise control of the porosity and refractive index of the spin-processed coating. Coating thickness measurements as a function of solution aging time and temperature allow for determination of the activation energy of the reaction-limited aggregation process. We demonstrate optimization of the antireflection effect for a single-layer silica nanoparticle coating on glass, and suggest that the aggregation method may be generalized to various other nanoparticle-based assemblies.

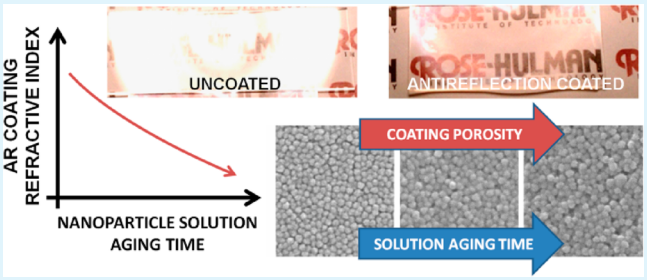

KEYWORDS: *nanoparticle, colloid, silica, antireflection, aggregation, thin films*

The performance of a single-layer antireflection (AR) coating can be optimized through careful control of the coating thickness and refractive index. Porous oxides have long been attractive for use as thin-film optical coatings because of their low cost, ease of preparation, and potential for index adjustment by varying the degree of porosity in the coating.[1−17] In this communication, we describe a straightforward one-step process for creating index- and thickness-tunable AR coatings from commercially available silica nanoparticle solutions that have been aged under conditions in which the silica nanoparticles undergo controllable aggregation in solution before application to a substrate via spin-coating. The extreme ease and flexibility of the process make it an attractive alternative to other types of sol−gel[5,8,10,14,17] and layer-by-layer[12,13,15,16] schemes that require more detailed procedures and longer processing times. In addition, we demonstrate that the aggregation and spin-coating process is a viable route for examining aggregation kinetics, including determining activation energies for the surface reactions that drive nanoparticle aggregation at near-neutral pH.

AR coating design and fabrication is a well-established yet very active field of research.[18] The high level of interest in the field is due to a number of factors, notably including the broadening range of optical technologies and materials to be coated, as well as the desire to include insights from nature into the design of biomimetic structures (e.g., "moth eye coatings") that differ structurally from the classical single- or multilple-layer coating approaches.[18,19] Nevertheless, more conventional coating approaches remain popular and technologically important due to their relative flexibility of design, low cost, and ease of fabrication.

Single-layer quarter-wave AR coatings are designed to suppress reflection of light at the interface between an ambient medium (typically air, $n_{air} = 1$) and a substrate (here glass slides, $n_{sub} = 1.56$). The coating causes deconstructive phase matching of beams reflected from the coating surface and the coating-substrate interface, resulting in enhanced transmission of light.[20] The minimum reflection of such coatings occurs at a wavelength $\lambda_{min} = 4n_c d$, where d, the thickness of the coating, is typically chosen so that λ_{min} is near the center of the visible spectrum ($\approx$ 550 nm). An AR coating is most effective when the refractive index of the coating is equal to the geometric mean of the ambient and substrate indices,[20] i.e., $n_c = (n_{air}n_{sub})^{1/2}$. For example, the glass slides in this work have $n \approx 1.56$, so an optimum coating index and thickness would be $n_c = \sqrt{n_{sub}} = 1.25$ and $d \approx 110$ nm. Optical elements are made from a variety of materials, however, and a versatile AR coating process would allow for tuning both the index and coating thickness to optimize the antireflection effect in a given system. In this communication, we spin coat solutions of silica nanoparticles to create porous silica coatings that naturally have n_c such that $1 < n_c < n_{silica}$ ($\approx$ 1.5). The principles we outline, however, could also be applicable to colloidal sols of higher index oxides such as TiO_2 that could be utilized to

Received: September 20, 2012
Accepted: December 3, 2012
Published: December 3, 2012

   dx.doi.org/10.1021/am3020586 | ACS Appl. Mater. Interfaces 2012, 4, 6426−6431

design coatings on higher index materials such as sapphire, diamond, and silicon.

Utilizing a commercially available silica nanoparticle solution (Ludox HS-30, 12 nm diameter), we first demonstrated thickness control by spin-coating aqueous dilutions of the stock solution onto silicon wafers, followed by measurements of the thickness and refractive indices of the resulting coatings using reflectometry and ellipsometry and assuming a single-layer Cauchy dispersion model (Figure 1a). All of these

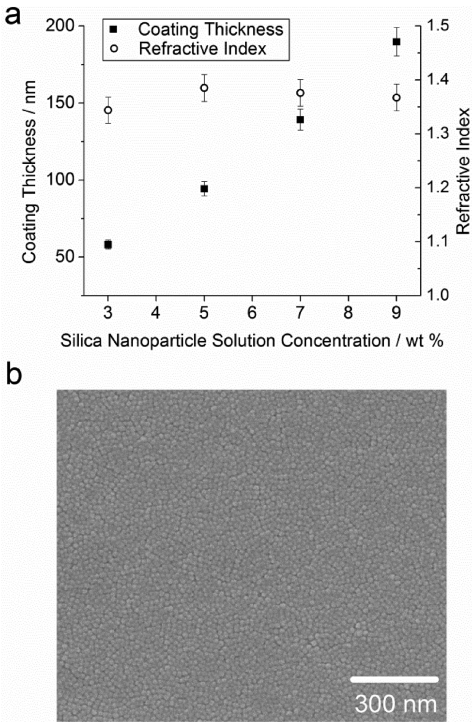

Figure 1. (a) Coating thickness (closed squares) and refractive index (open circles) for silica colloidal coatings on silicon as a function of the nanoparticle solution concentration. (b) SEM surface image of a coating illustrating the high density of particle packing.

coatings were found to be of excellent optical quality, being visually uniform in color and exhibiting no cracking or other major imperfections for any of the solution concentrations below 9 wt %. The lack of fracturing in these coatings upon drying during the spin coating process was a significant observation, as cracking is generally a difficult problem to overcome during solution processing of colloidal thin film systems.[21,22] We did observe cracks in thicker coatings produced from higher concentrations of silica, but the onset of cracking appeared in coatings too thick (>300 nm) to exhibit ideal AR behavior. The single-layer AR coatings in this work could be manufactured crack-free because their thicknesses were below the critical cracking thickness for the system, which is a parameter dependent upon the shear modulus of the particles, the water−air interfacial tension, and the volume packing fraction of the coating.[21] In related work, however, we have found that thicker crack-free coatings may be manufactured from successive spin-coating of thinner crack-free layers.[23] For the single-layer coatings in this work, Figure 1a shows a strong linear correlation between coating thickness and solution concentration; these data confirm that diluted nanoparticle solutions can be easily utilized to create coatings of a specified thickness. The coatings exhibited a constant refractive index (within measurement uncertainty) of $n_c \approx 1.37 \pm 0.02$ (single index values are reported at 633 nm) for all thicknesses, suggesting no major difference in particle packing for spin-coated coatings between approximately 60 and 200 nm in thickness.

Depending upon the type of effective medium model chosen (see the Supporting Information for more details), a measurement of $n_c = 1.37 \pm 0.02$ for these coatings implies a porosity of 19 − 23%. This value is lower than the value of 45% reported previously for all-SiO_2 nanoparticle coatings assembled via the layer-by-layer (LbL) method,[12] suggesting that the one-step spin coating approach described here leads to relatively low porosity coatings. This was confirmed by examining the surface of a spin coated sample in SEM (Figure 1b), which clearly showed a dense particle packing with localized regions of crystalline order. Figure 1b also reveals a small degree of polydispersity and irregularity in the particles comprising the coating; these observations may explain why our calculated porosity was lower than both the typical expected value for a random close packing of monodisperse spheres (36%), as well as the theoretically lowest possible porosity based on the hexagonal or face-centered close-packing of monodisperse spheres (26%). It is known that both polydispersity as well as deviations in shape of spherical particles can lead to increases in the expected packing density;[24] it appears that for our system both factors may play a role in forming a densely packed coating.

The ability to adjust (in particular, lower) the coating refractive index for a one-step spin-coated sample necessitated a strategy for preventing close packing of the nanoparticles during the coating drying step. We focused on inducing aggregation among the nanoparticles prior to spin deposition, with the expectation that irregularly shaped nanoparticle aggregates would prohibit the degree of close packing observed in diluted stock samples. The SiO_2 nanoparticles we utilized here are negatively charged in solution (pH ≈ 10); therefore, initial efforts to induce aggregation focused on the addition of positively charged flocculation agents including nanoparticles and polyelectrolytes at varying concentrations. Ultimately, these efforts failed to produce nanoscale flocs that could effectively decrease the coating index while maintaining good optical clarity.

Our next approach focused on simply lowering the pH of the silica stock solution to reduce the negative surface charge on the particles and induce aggregation through condensation reactions of surface hydroxyl groups. Silica nanoparticle solutions are known to possess nontrivial pH stability characteristics. Low pH values are catalytically unfavorable for the condensation of hydroxyl groups, while high pH values discourage particle collisions due to increased negative surface charge.[25] The result is that silica nanoparticle solutions tend to be least stable at near-neutral pH; consequently, to induce aggregation we adjusted 30 wt % silica stock solutions to pH 7.0 utilizing HCl and aged the solutions for a controlled amount of time at laboratory temperature (23 °C) before removing an aliquot of the aggregated nanoparticle solution and diluting it with water to a concentration of 5 wt % and spin coating onto a Si wafer. To evaluate the effect of temperature on the aggregation reaction and test whether it is possible to control the aggregation kinetics, we performed additional aggregation experiments at 4, 50, and 60 °C, in each case again removing aliquots of the stock solution at controlled time intervals, diluting to 5 wt %, and spin coating onto Si wafers.

The thickness and refractive indices of all coatings were measured using both spectroscopic ellipsometry and reflectometry, and the results are shown in Figure 2.

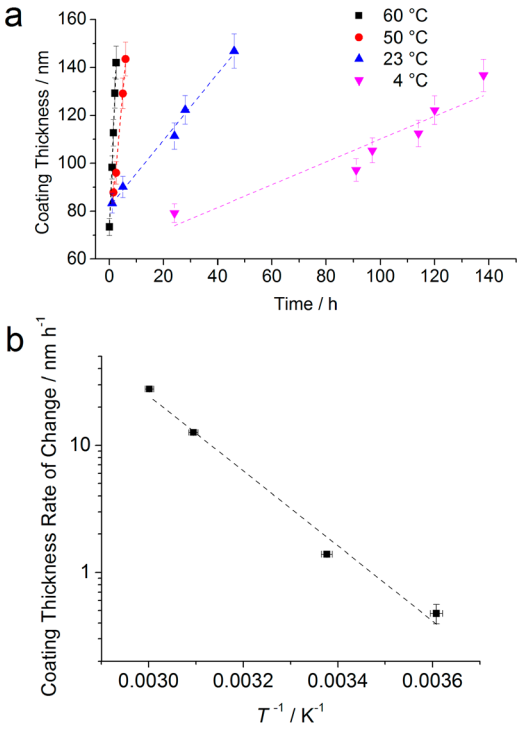

Figure 2. (a) Coating thickness versus aging time for solution aging temperatures (T) ranging from 4 to 60 °C. Coatings were spin coated from 5 wt % solutions onto silicon substrates. (b) Arrhenius plot of the coating thickness rate of change versus T^{-1}.

As illustrated in Figure 2a, the thickness of the aggregated particle coatings was a function of both the solution aggregation time and temperature. When allowing aggregation to proceed in solution at a given temperature, the resulting coating thickness from spin-coated aliquots increased linearly with the time at which the solution was sampled, exhibiting an R-squared correlation coefficient >0.99 for the three highest temperatures. At 4 °C, an approximate linear trend was still evident, but the correlation coefficient decreased to 0.89. The fact that all samples were prepared by spin coating from solutions of the same concentration suggested that the increase in coating thickness was due to the spin deposition of sol aggregates of increasing size and decreasing ability to pack densely within the coating. The apparent linear trend in coating thickness with time led us to hypothesize that the rate of change in coating thickness at a given temperature may in turn reflect the kinetics of the aggregation process. Plotting the slope of the coating thickness versus time data from Figure 2a as a function of inverse temperature revealed an Arrhenius-type relationship with R-squared = 0.99 (Figure 2b). The activation energy (E_a) determined from the slope of the correlation line was 57 ± 10 kJ/mol. This value is within the range of E_a values (32 to 69 kJ/mol) reported previously for silica sol aggregation processes,[25] making it reasonable to assume that the increase in coating thickness with time does indeed reflect the aggregation kinetics of the silica particles. This conclusion was further corroborated by dynamic light scattering (DLS) measurements of aggregate size as a function of temperature and time (see the Supporting Information, Figure S1a); these data confirmed an increase in hydrodynamic diameter of aggregates in solution as a function of time. The DLS data confirm an exponential functional dependence of the aggregate diameter as a function of aging time at a given temperature, which is expected for a reaction-limited aggregation process.[26,27] Moreover, the activation energy of the kinetic rate constant deduced from DLS-measured aggregate growth (55 ± 5 kJ/mol) agreed very closely with the number we obtained from the coating thickness data. Interestingly, an exponential-type growth of hydrodynamic radius for solution-phase aggregates translates into a linear-type growth rate of spin-processed coatings, the origin of which warrants further study.

Figure 3 provides further evidence that the increase in coating thickness shown in Figure 2a is strongly correlated with

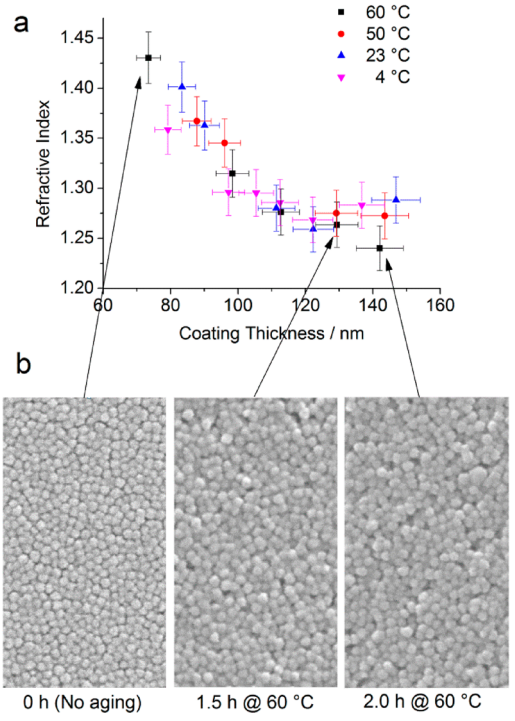

Figure 3. (a) Refractive indices of the coatings from Figure 2a plotted versus their thicknesses. (b) SEM surface images of coatings spin-coated from 5 wt % solutions of samples aged at 60 °C for the indicated times. Arrows to part a indicate samples with identical aging conditions. Each panel in b is 300 nm wide.

a decrease in coating density. As illustrated in Figure 3a, the refractive index of all coatings decreased with increasing thickness. When plotted versus coating thickness, the refractive index measurements for all coatings appeared to fall along a common curve. For early aging times the coating index exhibited a strong, decreasing linear relationship with coating thickness from a value of n > 1.4 (for a thickness of 73 nm) for unaged solution to a value of $n \approx 1.26$ for thicknesses approaching 110 nm. The refractive index exhibited an apparently negligible dependence on solution aging temperature in this early aging regime. When the coating thickness increased above 110 nm the refractive index appeared to level out and perhaps even increase slightly for the lowest aging temperatures, exhibiting no further measurable decrease for coating thicknesses up to approximately 150 nm. An exception was the sample aged at 60 °C, for which the index appeared to decrease further, if only slightly, to a value of 1.24. Solutions

dx.doi.org/10.1021/am3020586 | ACS Appl. Mater. Interfaces 2012, 4, 6426–6431

aged further at all temperatures began to gel, which prevented redispersion of the nanoparticles for spin coating.

To examine the morphology of coatings produced following the solution aging process, we obtained SEM images of the surfaces of three samples: one spin-coated from unaged solution, and two spin-coated from solutions aged at 60 °C for times of 1.5 and 2 h, respectively; these results are shown in Figure 3b, with arrows indicating samples on the refractive index plot (Figure 3a) that had identical preparations. While the unaged sample reflects the same dense-packed structure shown in Figure 1b, the micrographs of samples aged for 1.5 and 2 h at 60 °C reveal a less dense packing structure with a more textured surface, greater spacing between particles, and substantial void spaces within the coating. We note that techniques such as atomic force microscopy would be capable of quantitatively characterizing the surface topology, and may conceivably be used to improve optical modeling of coatings by providing information, for example, about the surface roughness of the coating. As indicated previously, however, single-layer optical models provided excellent fits for the data, and we assumed that the effective refractive index for the furthest time point at each aging temperature could be used with an effective medium approximation (EMA) to calculate the lowest possible porosity for an AR coating constructed using this technique.

A number of EMAs have been proposed for multiphase coatings containing various dispersed-phase materials and geometries.[28] Here, we examined three: the simple weighted index (Birchak)[29] and weighted dielectric (Yoldas)[30] models, and the symmetric Bruggeman model.[18,28,31] (see the Supporting Information for more details). These data are shown in Table 1, where it can be seen that the weighted index and Bruggeman models are in excellent agreement, while the weighted dielectric model suggests slightly higher porosity values. Nevertheless, the models considered here do not differ in their porosity predictions for any sample by more than 5%.

Table 1. Ultimate Refractive Index and Calculated Porosity (using three different effective medium models) of Colloidal Coatings As a Function of Solution Aging Temperature

solution aging temperature (°C)	refractive index	porosity (%)[a]	porosity (%)[b]	porosity (%)[c]
4	1.28 ± 0.02	39 ± 5	38 ± 5	44 ± 6
23	1.29 ± 0.02	37 ± 5	36 ± 5	41 ± 6
50	1.27 ± 0.02	41 ± 5	40 ± 5	46 ± 5
60	1.24 ± 0.02	48 ± 5	46 ± 5	52 ± 5

[a]Porosity calculated assuming the weighted index (Birchak) model. [b]Porosity calculated assuming the symmetric Bruggeman model. [c]Porosity calculated assuming the Yoldas, or fractionally weighted dielectric constant model (see the Supporting Information for more details).

To evaluate the ability of the aging process to improve the AR effect, we spin-deposited 5 wt % nanoparticle coatings taken as dilutions from both aged (2 h at 60 °C) and unaged solutions onto transparent glass substrates (both sides) and measured the reflectance of the samples. Parallel measurements of the transmittance of similarly prepared coatings were performed; the transmittance measurements confirmed that the decrease in reflectance was due to enhanced light transmission and not diffuse scattering (see the Supporting Information for more details). Figure 4 demonstrates that although both coatings decreased the double-sided reflectance

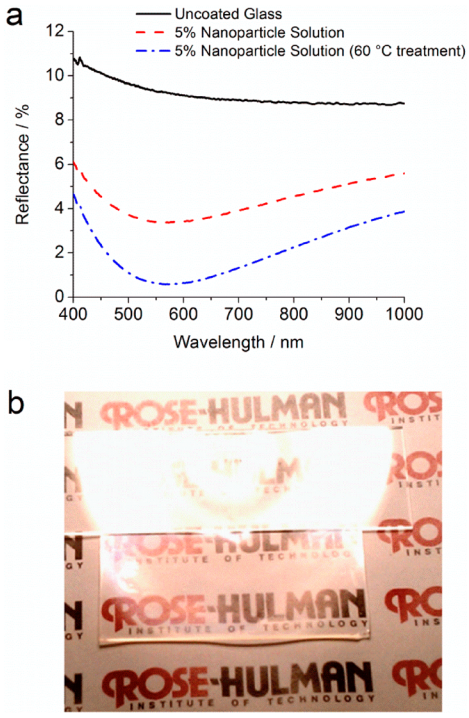

Figure 4. (a) AR performance of coatings (double-sided on glass slides) created by spin-coating a 5 wt % dilution of the unaged solution (dashed line) and a 5 wt % dilution of a solution aged at 60 °C for 2 h (dashed-dotted line). The reflectance of the uncoated glass is shown as the solid line for comparison. (b) Photo of an uncoated glass slide (top) next to a double-sided aged AR coating (bottom) under direct reflected light from an overhead lamp.

of the bare glass (which was between 9 and 10% over the visible part of the spectrum), the glass slide coated from the aged solution exhibited a reflectance minimum below 1%, in contrast to a minimum reflectance of approximately 4% for a coating produced from an unaged solution (Figure 4a). Interestingly, the reflectance minima occurred at roughly the same wavelength (567 nm for aged, 573 nm for unaged), indicating that the two coatings had very comparable optical thicknesses (the product of the refractive index and thickness). This is due to the fact that the decrease in refractive index exhibited by coatings prepared from aged solutions (Figure 3a) happens concomitantly with an increase in coating thickness (Figure 2a). The lower index of the aged coating, however, is more closely matched to the square root of the refractive index of the glass slide, allowing for better AR performance. The photograph in Figure 4b, which was taken under direct reflected light, illustrates the AR capabilities of our aged AR coatings; a bare glass slide is shown next to a glass slide prepared with the aged coating. The latter sample strongly suppresses reflection, causing a decrease in glare and an enhancement in transparency that allows for easy viewing of the text beneath the sample.

The approach that we have described in this work offers some significant advantages in comparison to previous work for tuning the refractive index of nanoparticle coatings for AR applications. Although pH-mediated aggregation has been proposed before as a viable method for decreasing the index of particle coatings,[1,3] this is the first work to our knowledge to demonstrate a clear connection between aggregate growth kinetics and the resulting coating thickness. Although certain synthesis techniques are able to generate mesoporous or hollow

dx.doi.org/10.1021/am3020586 | ACS Appl. Mater. Interfaces 2012, 4, 6426−6431

particles with naturally low refractive indices,[2,4,5,13] most strategies aimed at tuning the coating index over a wider range using conventional amorphous silica particles (such as the type that are widely available commercially) appear to exhibit relatively narrow variations in index, or are tunable over a range inappropriate for the majority of glass and polymer substrates.[6,7,10] The above-mentioned references are largely variations on spin- or dip-processing of nanoparticle solutions. Other techniques such as layer-by-layer assembly[12,13,15,16] and spin-on sol−gel precursor processing[5,8,10,14,17] have shown significant promise for generating coatings with tunable properties and greater coating complexity. Unfortunately, the greater complexity of these techniques pushes processing time from seconds to minutes or even hours, and can mean the introduction of nonaqueous solvents, which may be incompatible with certain substrates (e.g., plastics) or be undesirable from an environmental standpoint.

Although it could be less important in certain instances (e.g., internal optical elements), future work is needed to evaluate the mechanical properties of these coatings to ensure their amenability to the broadest possible range of applications. Nanoindentation[32] and mechanical abrasion testing[33] have become popular testing methods for nanoparticle coatings, and various means have been proposed to increase nanoparticle coating durability.[32−34] Besides mechanical concerns, long-term stability of the AR performance of these coatings requires that they do not substantially change their thickness or refractive index over time. We have noted preliminarily that the optical properties of these coatings appear stable over at least a period of several weeks, although the effective refractive index appears to vary directly with the ambient relative humidity, presumably as water condenses within the pore structure of the coating. We are currently investigating modifications to the internal surface chemistry of the porous coatings in order to affect the degree to which water could either be attracted to or repelled from the pores, e.g., for sensing applications[31] or maintaining constant optical properties, respectively.

In summary, we have demonstrated that controlled aggregation of pH-neutralized silica nanoparticle solutions followed by spin coating provides a straightforward method to fabricate single-layer AR coatings. The speed and extent of nanoparticle aggregation can be controlled by varying the temperature and duration of the solution aging process; longer aging times lead to thicker coatings with lower refractive indices, suggesting that aggregated nanoparticles cannot pack as densely within the coating. At a given temperature, the extent of aggregation can be monitored by observing the thickness increase of spin-processed coatings over time. Comparison of such data at several temperatures suggests that the aggregation kinetics follow an Arrhenius relationship with $E_a = 57 \pm 10$ kJ/mol, which agrees well with previous reports. Coatings produced from aged solutions on glass slides had significantly better AR performance than coatings applied directly from unaged nanoparticle solutions. The technique outlined in this paper is particularly promising due to the ability to directly process particle coatings with tunable refractive index and thickness; furthermore, we believe the approach presented in this study can be extended to other types of oxide nanoparticles to form highly porous coatings for various applications including optics, photonics, and energy storage and conversion.

■ ASSOCIATED CONTENT

Supporting Information

Experimental details, porosity calculations, dynamic light scattering analysis, and comparison of reflection and transmission measurements. This material is available free of charge via the Internet at http://pubs.acs.org.

■ AUTHOR INFORMATION

Corresponding Author

*E-mail: nolte@rose-hulman.edu.

Notes

The authors declare no competing financial interest.

■ ACKNOWLEDGMENTS

A.J.N. and K.T.C. gratefully acknowledge Prof. Maarij Syed of Rose-Hulman for assistance with ellipsometry, and financial support from the NSF Science and Technology Center for Layered Polymeric Systems (Grant 0423914). D.L. and K.E.T. acknowledge support from NSF (DMR-1055594) and the Penn MRSEC (NSF DMR-1120901).

■ REFERENCES

(1) Cathro, K.; Constable, D.; Solaga, T. *Solar Energy* **1984**, *32*, 573−579.
(2) Thomas, I. M. *Appl. Opt.* **1986**, *25*, 1481−1483.
(3) Pettit, R. B.; Ashley, C. S.; Reed, S. T.; Brinker, C. J. In *Sol−Gel Technology for Thin Films, Fibers, Preforms, Electronics and Specialty Shapes*; Klein, L. C., Ed.; William Andrew Publishing/Noyes: Park Ridge, NJ, 1988; p 80.
(4) Thomas, I. M. *Appl. Opt.* **1992**, *31*, 6145−6149.
(5) Biswas, P. K.; Devi, P. S.; Chakraborty, P. K.; Chatterjee, A.; Ganguli, D.; Kamath, M. P.; Joshi, A. S. *J. Mater. Sci. Lett.* **2003**, *22*, 181−183.
(6) Prevo, B. G.; Hwang, Y.; Velev, O. D. *Chem. Mater.* **2005**, *17*, 3642−3651.
(7) Krogman, K. C.; Druffel, T.; Sunkara, M. K. *Nanotechnology* **2005**, *16*, S338−S343.
(8) Choi, S. Y.; Mamak, M.; Von Freymann, G.; Chopra, N.; Ozin, G. A. *Nano Lett.* **2006**, *6*, 2456−2461.
(9) Yancey, S. E.; Zhong, W.; Heflin, J. R.; Ritter, A. L. *J. Appl. Phys.* **2006**, *99*, 034313.
(10) Vincent, A.; Babu, S.; Brinley, E.; Karakoti, A.; Deshpande, S.; Seal, S. *J. Phys. Chem. C* **2007**, *111*, 8291−8298.
(11) Hoshikawa, Y.; Yabe, H.; Nomura, A.; Yamaki, T.; Shimojima, A.; Okubo, T. *Chem. Mater.* **2010**, *22*, 12−14.
(12) Lee, D.; Gemici, Z.; Rubner, M. F.; Cohen, R. E. *Langmuir* **2007**, *23*, 8833−8837.
(13) Du, Y.; Luna, L. E.; Tan, W. S.; Rubner, M. F.; Cohen, R. E. *ACS Nano* **2010**, *4*, 4308−4316.
(14) Uhlmann, D. R.; Suratwala, T.; Davidson, K.; Boulton, J. M.; Teowee, G. *J. Non-Cryst. Solids* **1997**, *218*, 113−122.
(15) Lee, D.; Rubner, M. F.; Cohen, R. E. *Nano Lett.* **2006**, *6*, 2305−2312.
(16) Shimomura, H.; Gemici, Z.; Cohen, R. E.; Rubner, M. F. *ACS Appl. Mater. Interfaces* **2010**, *2*, 813−820.
(17) Faustini, M.; Nicole, L.; Boissiére, C.; Innocenzi, P.; Sanchez, C.; Grosso, D. *Chem. Mater.* **2010**, *22*, 4406−4413.
(18) Raut, H. K.; Ganesh, V. A.; Nair, A. S.; Ramakrishna, S. *Energy Environ. Sci.* **2011**, *4*, 3779−3804.
(19) Huang, Y.-F.; Chattopadhyay, S.; Jen, Y.-J.; Peng, C.-Y.; Liu, T.-A.; Hsu, Y.-K.; Pan, C.-L.; Lo, H.-C.; Hsu, C.-H.; Chang, Y.-H.; Lee, C.-S.; Chen, K.-H.; Chen, L.-C. *Nat. Nanotechnol.* **2007**, *2*, 770−774.
(20) Heavens, O. S. In *Optical Properties of Thin Solid Films*; Dover Publications: New York, 1965; p 209.
(21) Singh, K. B.; Tirumkudulu, M. S. *Phys. Rev. Lett.* **2007**, *98*, 218302.

(22) Tirumkudulu, M. S.; Russel, W. B. *Langmuir* **2005**, *21*, 4938−4948.
(23) Prosser, J. H.; Brugarolas, T.; Lee, S.; Nolte, A. J.; Lee, D. *Nano Lett.* **2012**, *12*, 5287−5291.
(24) Donev, A.; Cisse, I.; Sachs, D.; Variano, E. A.; Stillinger, F. H.; Connelly, R.; Torquato, S.; Chaikin, P. M. *Science* **2004**, *303*, 990−993.
(25) Iler, R. K. In *The Chemistry of Silica: Solubility, Polymerization, Colloid and Surface Properties, and Biochemistry*; Wiley: New York, 1979; pp 366−369.
(26) Weitz, D. A.; Huang, J. S.; Lin, M. Y.; Sung, J. *Phys. Rev. Lett.* **1985**, *54*, 1416−1419.
(27) Lin, M. Y.; Lindsay, H. M.; Weitz, D. A.; Ball, R. C.; Klein, R.; Meakin, P. *Phys. Rev. A* **1990**, *41*, 2005−2020.
(28) Hutchinson, N. J.; Coquil, T.; Navid, A.; Pilon, L. *Thin Solid Films* **2010**, *518*, 2141−2146.
(29) Birchak, J. R.; Gardner, C. G.; Hipp, J. E.; Victor, J. M. *Proc. IEEE* **1974**, *62*, 93−98.
(30) Díaz-Parralejo, A.; Caruso, R.; Ortiz, A. L.; Guiberteau, F. *Thin Solid Films* **2004**, *458*, 92−97.
(31) Calvo, M. E.; Colodrero, S.; Hidalgo, N.; Lozano, G.; López-López, C.; Sánchez-Sobrado, O.; Míguez, H. *Energy Environ. Sci.* **2011**, *4*, 4800−4812.
(32) Dafinone, M. I.; Feng, G.; Brugarolas, T.; Tettey, K. E.; Lee, D. *ACS Nano* **2011**, *5*, 5078−5087.
(33) Gemici, Z.; Shimomura, H.; Cohen, R. E.; Rubner, M. F. *Langmuir* **2008**, *24*, 2168−2177.
(34) Zhang, L.; Prosser, J. H.; Feng, G.; Lee, D. *Nanoscale* **2012**, *4*, 6543−6552.